Effect of octupole deformation of fragments on mass-asymmetric yields of fission of actinide nuclei

Dong-ying Huo,[1] Zheng Wei,[1,2,*] Kang Wu,[1] Chao Han,[1] Ya-ning Han,[1] Yi-xuan Wang,[1] Peng-qi Zhang,[1] Yuan He,[3] Xiao-jun Bao,[4] Zhi-yong Deng,[1,5] and Ze-en Yao[1,2]

[1]*School of Nuclear Science and Technology, Lanzhou University, 730000 Lanzhou, China*

[2]*Engineering Research Center for Neutron Application Technology, Ministry of Education, Lanzhou University, 730000 Lanzhou, China*

[3]*School of Mathematics and Statistics, Lanzhou University, Lanzhou 730000, China*

[4]*Department of Physics, Hunan Normal University, 410081 Changsha, China*

[5]*Nuclear Power Institute of China, 610000 Chengdu, China*

(Received 21 May 2023; revised 3 July 2023; accepted 1 August 2023; published 21 August 2023)

The yield distributions of neutron-induced fission of actinides were calculated and evaluated by using the improved scission-point model with considering octupole deformation of fragments. We studied the influence of the octupole deformation on the asymmetric yields of actinides fission. The more probable scission configuration is the pear-shaped heavy fragments rather than more spherical shape. We used the improved scission model to calculate the peak of charge and neutron distributions and compared results with the experimental data. The results confirm that the main asymmetric fission mode of the heavy actinides fission is indeed characterized by "$Z_H \approx 54$." The protons configuration of heavy fragment plays a dominant role in asymmetric fission of actinides.

DOI: 10.1103/PhysRevC.108.024608

I. INTRODUCTION

Since the phenomenon of neutron-induced fission of uranium was discovered in 1938, research has been going on the process of nuclear fission. In particular, actinides are important nuclear fuel for fission devices, and its fission yields data are the key to determining burnup and transmutation system [1]. The model of actinides fission is mainly by asymmetric splitting including mass distributions and charge distributions, shown as bimodal shape, especially, low excitation energy.

The scission point model as a typical statistical method can calculate and reproduce yield distributions [2–9]. The potential at the scission point is essentially given by the liquid-drop (LD) energy and shell energies of proton and neutron subsystems of the two nascent fragments and their interaction. The strong shell effects occur in spherical nuclear, so the strongest shell energy of double magic nuclei ^{132}Sn can affect the peak position on mass distributions of fission heavy fragments. Andreev *et al.* developed the scission point model by the better definition of the scission configuration and by the inclusion of the deformations of the fission fragments, which can be used to calculate the yield distributions of fragment in the neutron-induced fission of the actinide nuclide and predict the excitation energy dependencies of the asymmetric and symmetric fission modes [10,11]. However, the accuracy of calculated yields distributions data needs to be further improved.

The fission fragments will deform under strong interactions at the scission point, and previous statistical models assumed that the shapes of most heavy nuclei are characterized by spherical and quadrupole deformed nuclei [10–12]. But, in recent years, experiments have identified stable octupole-deformed nuclei in the ground state, such as ^{144,146}Ba [13–15], which give evidence of occurring pear-shaped fission fragments at low energies. In the recent work, the authors confirmed demonstrably that the elongated deformed compound nucleus exhibit strong octupole shapes before scission [16]. They consider that although spherical shell effects in the ^{132}Sn ($Z = 50$) are often considered as a driver for the formation of the heavy fragments, which is also determined by the extra stabilized octupole deformation nucleus ^{144}Ba ($Z = 56$). The shell-stabilized deformation can drive the fission dynamics toward neutron and proton numbers between the double magic ^{132}Sn ($N = 82$, $Z = 50$) and shaped ^{144}Ba ($Z = 56$, $N = 88$).

In this paper, the scission point model is further improved by adding the octupole deformations of the fission fragments. The improved scission point model can calculate the mass distributions of neutron-induced actinides fission with low incident neutron energy. We also given a reasonable explanation from quantum shells. The more probable scission configuration is the pear-shaped heavy fragments rather than more spherical shape. We further studied the role of shells in the asymmetric split in the actinides, the results suggest the position of the heavy component is constant at $Z_H \approx 54$ and has larger movement in neutron number. This indicates that the shell effect of proton number plays a more important role in asymmetric fission than previously thought.

This article is organized as follows: Sec. II is devoted to our model briefly. The discussion is given on the results obtained by considering octupole deformations of fragments in Sec. III. The calculations and discussions of the mass yields are given in Sec. IV. Finally, in Sec. IV, we will give a summary.

*Corresponding author: weizheng@lzu.edu.cn

II. METHODS

The basic assumption of the scission point model is that statistical equilibrium is established at the scission where the observable characteristics of fission process are formed. When the deformation is large enough, the parent fissioning nucleus splits into a pair of nearly touching coaxial daughter nuclei. To simplify, we have adopted axial symmetry deformations (β_{2i}, β_{3i}). The index i $(i = L, H)$ designates the light or heavy fragment.

The fission fragment distribution is determined by the relative potential energy of a given fragmentation combinations at the scission point. The potential energy consists of binding energy of the light (L) and heavy (H) fragments with the mass numbers A_L (A_H) and charge numbers Z_L (Z_H), as well as Coulomb potential and nuclear potential between two fragments. The potential energy U at the scission point as a function of the deformations and the internuclear distance R between fragments is described as

$$\begin{aligned} &U(A_i, Z_i, \beta_i, R) \\ &\quad = B(A_L, Z_L, \beta_{2L}, \beta_{3L}, E_L^*) \\ &\qquad + B(A_H, Z_H, \beta_{2H}, \beta_{3H}, E_H^*) - B(A, Z, \beta_2, \beta_3, E^*) \\ &\qquad + V_C(A_i, Z_i, \beta_{2i}, \beta_{3i}, R) + V_N(A_i, Z_i, \beta_{2i}, \beta_{3i}, R), \end{aligned} \tag{1}$$

where $A = A_L + A_H$ $(Z = Z_L + Z_H)$ is the mass (charge) number of the fissioning nucleus. The deformation parameters are $\beta_{\lambda i}$, where $(\lambda = 2, 3;\ i = L, H)$ denote quadrupole and octupole deformations of the light and heavy fragments, respectively.

The binding energies $B(A_i, Z_i, \beta_{2i}, \beta_{3i}, E_i^*)$ as a function of quadrupole β_{2i} and octupole β_{3i} deformations are calculated by using the macroscopic microscopic method [17–19]. The binding energy of each fragment consists of the LD energy $U^{\rm LD}$, the shell correction energy $\delta U^{\rm shell}$. The LD energy is calculated as $U^{\rm LD} = E^{\rm LD}(A, Z)\prod_{\lambda=2}(1 + b_\lambda \beta_\lambda^2)$, the dependence of b_λ on the mass number can be reasonably well described by the formula in Ref. [17]. The energy of a spherical nucleus is described a Bethe-Weizsäcker mass formula,

$$\begin{aligned} E^{\rm LD}(A, Z) = &-15.5841A + 18.2359A^{2/3} \\ &+ 0.7173\frac{Z(Z-1)}{A^{1/3}}(1 - Z^{-2/3}) \\ &+ a_{\rm sym}I^2A - 5.5108A^{-1/3}\delta_{np}, \end{aligned} \tag{2}$$

with isospin asymmetry $I = (N - Z)/A$. The expression of δ_{np} depends on the values of the proton number and neutron number, express as

$$\delta_{np} = \begin{cases} 2 - |I| & N \text{ and } Z \text{ even} \\ |I| & N \text{ and } Z \text{ odd} \\ 1 - |I| & N \text{ enen, } Z \text{ odd, and } N > Z \\ 1 - |I| & N \text{ odd, } Z \text{ even, and } N < Z \\ 1 & N \text{ enen, } Z \text{ odd, and } N < Z \\ 1 & N \text{ odd, Z even, and } N > \text{Z} \end{cases}. \tag{3}$$

The symmetry energy coefficient of finite nuclei is written as

$$a_{\rm sym} = 29.2876\left[1 - \frac{1.4492}{A^{1/3}} + \frac{2 - |I|}{2 + |I|A}\right]. \tag{4}$$

The influence of excitation energy on mass distributions results from the tricky competition between the macroscopic LD energies and the microscopic shell corrections at scission. The shell correction is obtained by the traditional Strutinsky procedure, which is the sum of shell energies of protons and neutrons [20].

The damping of shell correction with excitation energy is introduced as

$$\begin{aligned} &\delta U^{\rm shell}(A_i, Z_i, \beta_{2i}, \beta_{3i}, E_i^*) \\ &\quad = \delta U^{\rm shell}(A_i, Z_i, \beta_{2i}, \beta_{3i}, E_i^* = 0)\exp(-E_i^*/E_D), \end{aligned} \tag{5}$$

where E_D is the damping constant meaning the speed of washing out the shell correction against the excitation energy.

The interaction potential consists of the Coulomb potential V_C and nuclear potential V_N. The Coulomb interaction can be calculated by using Wong's formula [21],

$$\begin{aligned} V_C(R) = &\frac{Z_L Z_H e^2}{R} \\ &+ \left(\frac{9}{20\pi}\right)^{1/2}\frac{Z_L Z_H e^2}{R^3}\sum_{i=L,H}\left[R_i^2\beta_{2i}p_2(\cos\theta_i)\right] \\ &+ \frac{3}{7\pi}\frac{Z_L Z_H e^2}{R^3}\sum_{i=L,H}\left\{R_i^2[\beta_{2i}p_2(\cos\theta_i)]^2\right\} \\ &+ \left(\frac{9}{28\pi}\right)^{1/2}\frac{Z_L Z_H e^2}{R^4}\sum_{i=L,H}\left[R_i^3\beta_{3i}p_3(\cos\theta_i)\right] \\ &+ \frac{3}{7\pi}\frac{Z_L Z_H e^2}{R^4}\sum_{i=L,H}\left\{R_i^2[\beta_{3i}p_3(\cos\theta_i)]^2\right\}. \end{aligned} \tag{6}$$

The nuclear potential [22] is expressed as the double-folding form

$$\begin{aligned} &V_N(\beta_L, \theta_L, \beta_H, \theta_H, R) \\ &\quad = C_0\left\{\frac{F_{\rm in} - F_{\rm ex}}{\rho_{00}}\left(\int \rho_L^2(R)\rho_H(R - R_L)dR\right.\right. \\ &\qquad \left.\left. + \int \rho_L\rho_H^2(R - R_L)dR\right)\right. \\ &\qquad \left. + F_{\rm ex}\int \rho_L(R)\rho_H(R - R_H)dR\right\}, \end{aligned} \tag{7}$$

where, $F_{\rm in,ex} = f_{\rm in,ex} + f'_{\rm in,ex}\frac{N_L - Z_L}{A_L}\frac{N_H - Z_H}{A_H}$, $C_0 = 300$ MeV $\cdot$ fm^3, $f_{\rm in} = 0.09$, $f_{\rm ex} = -2.59$, $f'_{\rm in} = 0.42$, $f'_{\rm ex} = 0.54$ and $\rho_{00} = 0.16\,{\rm fm}^{-3}$. The nuclear density distribution of nuclei ρ_L and ρ_H can be, respectively, distributed in Woods-Saxon as

$$\rho_L(r) = \frac{\rho_{00}}{1 + \exp((r - R_L(\beta_L))/a]}, \tag{8}$$

$$\rho_H(r) = \frac{\rho_{00}}{1 + \exp((|r - R| - R_H(\beta_H))/a]}, \tag{9}$$

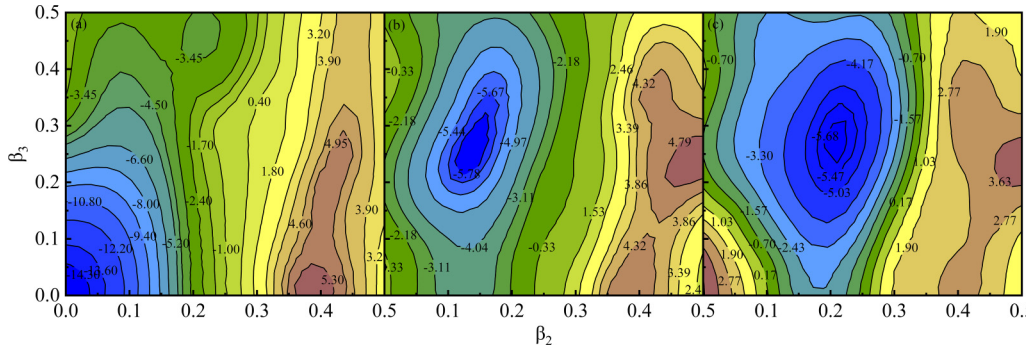

FIG. 1. The dependence of shell corrections of (a) ^{132}Sn, (b) ^{140}Xe, and (c) ^{144}Ba on the quadrupole and octupole deformation parameters.

where $a = 0.52$ fm represents the diffuseness parameter. The multipole expansion of the nuclear radius R_i of fragments is described in spherical coordinates as

$$R_i(\alpha_i) = c(\beta_{\lambda i})R_{0i}\left[1 + \sum_{\lambda=2,3} \beta_{\lambda i} Y_\lambda^0(\alpha)\right], \tag{10}$$

where $c(\beta_{\lambda i})$ is an essential parameter on the premise of the volume conservation. R_{0i} is the radius of the spherical nucleus. R corresponds to the $R_m = R_L + R_H + 0.5$ fm at which the potential pocket takes the minimum value of the interaction potential [22].

The relative formation probability w with fragments of certain charge numbers, mass numbers and deformations can be described as

$$w(A_i, Z_i, \beta_{2i}, \beta_{3i}, E^*) = \exp\left[-\frac{U(A_i, Z_i, \beta_{2i}, \beta_{3i}, R_m)}{T}\right]. \tag{11}$$

The temperature is calculated as $T = \sqrt{E^*/a}$, where $a = A/12\,\mathrm{MeV}^{-1}$ [22] is the level-density parameter in the Fermi-gas model. The excitation energy at scission is the initial excitation $E^*_{\mathrm{CN}}(E^*_{\mathrm{CN}} = E_n + Q)$ minus the potential-energy $U(A_i, Z_i, \beta_i, R_m)$, which is expressed as

$$E^*(A_i, Z_i, \beta_i, R_m) = E^*_{\mathrm{CN}} - U(A_i, Z_i, \beta_i, R_m). \tag{12}$$

Here, E_n is the neutron kinetic energy, and Q is the reaction energy. β_{2i} and β_{3i} should be integrated over to acquire the mass-charge distribution of the fission fragments yields, which is expressed as

$$Y(A_i, Z_i, E^*) = \int d\beta_{2L} d\beta_{2H} d\beta_{3L} d\beta_{3H}\, w(A_i, Z_i, \beta_{2i}, \beta_{3i}, E^*). \tag{13}$$

Eventually, the total mass distributions of the fission fragments should be normalized to 200% by definition. N_0 is the normalization constant. The mass and charge distributions (13) can be evolved into

$$Y(A_i, E^*) = N_0 \sum_{Z_i} Y(A_i, Z_i, E^*),$$
$$Y(Z_i, E^*) = N_0 \sum_{A_i} Y(A_i, Z_i, E^*). \tag{14}$$

III. OCTUPOLE DEFORMATION DURING FISSION

Nuclear fission of most actinides is dominated by asymmetric modes with charge distribution of the heavy fragments concentrated around proton numbers $Z \approx 54$, which indicates that ^{132}Sn is not the only driver on the way to fission. In this section, the main purpose is to analyze the influence of the shell-stabilized octupole deformation on potential energy affecting the scission-point configuration with the example of the ^{235}U fission.

Our calculation results in Sec. IV confirm that the peak position of the mass distribution of ^{236}U fission is around $A = 140$. Figure 1 shows the dependence of shell correction of ^{132}Sn (a), ^{140}Xe (b), and ^{144}Ba (c) on the quadrupole and octupole deformation parameters. The results are for regular nuclei not fission fragments at scission that are connected through a neck. With the increase in octupole deformation, lower shell correction can be obtained for ^{140}Xe and the minimum can be obtained at $\beta_2 = 0.15$, $\beta_3 = 0.25$. Hence, fragments ^{140}Xe exhibit a significant octupole deformation under strong nuclear force interaction at the scission point. This conclusion is not surprising since the neutron-rich even-even ^{140}Xe nucleus with $Z = 54$, $N = 86$ is located at the

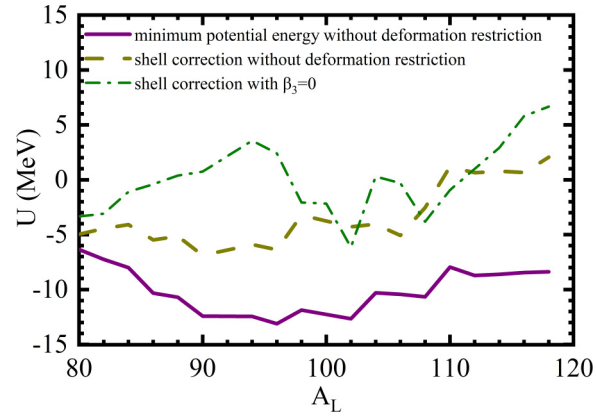

FIG. 2. The potential energy including the minimum potential energy without deformation restriction (purple solid line) and the sum of shell correction energy of light and heavy fragments without deformation restriction (green dotted line) and $\beta_3 = 0$ (green dot-dashed line) as a function of light-fragment mass number for neutron-induced fission of ^{235}U at temperature $T = 0$.

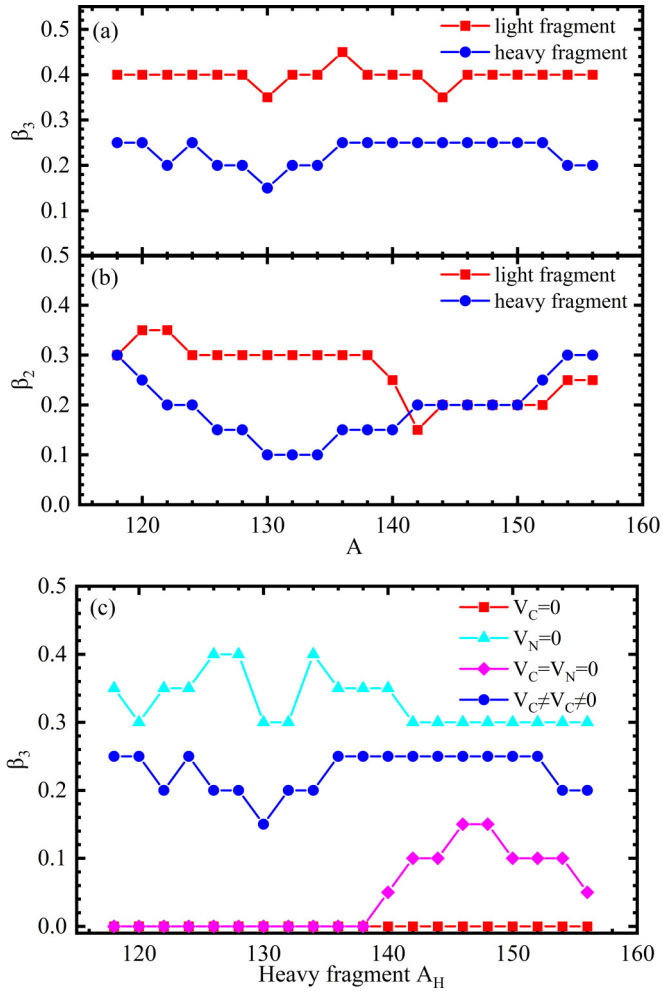

FIG. 3. The (a) quadrupole and (b) octupole deformations of scission configurations as a function of mass number for neutron-induced fission of ^{235}U at temperature $T = 0$. The relationship (c) between the octupole deformations of heavy fragments and the interaction potential energy by setting $V_N = 0$, $V_C = 0$, $V_C = V_N = 0$ and without limiting the interaction $V_C \neq V_N \neq 0$ at temperature $T = 0$.

lower edge octupole deformed island [23] of ^{144}Ba nucleus with the $Z = 56$, $N = 88$. They have similar shell structure as shown in Figs. 1(b) and 1(c). Although the LD energy tends to form the combination with less asymmetric fragments. The shell gaps nearer to symmetric splits will have more effect than those further away in both same shell gaps. Hence, this large gaps of octupole deformation are indeed expected to favor the formation of ^{140}Xe ($Z = 54$, $N = 86$) rather than ^{144}Ba ($Z = 56$, $N = 88$). In contrast, the spherical magic nuclei ^{132}Sn resists octupole deformation, which prevents its production as a fission fragment. The shell effects in double-magic nuclei ^{132}Sn show a weak influence at the strong deformation. This provides explanation for the favored production of ^{96}Sr + ^{140}Xe in neutron-induced ^{235}U fission.

Figure 2 shows the minimum potential energy and corresponding sum of shell correction energy of fragments configuration as a function light-fragments mass number.

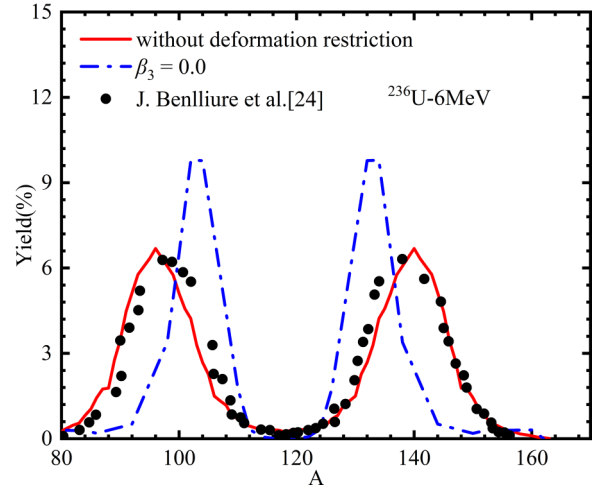

FIG. 4. Comparison between the calculated mass distributions for fission of ^{235}U by neutron at $\beta_3 = 0$ (blue dashed line) and without deformation restriction (red solid line). The experimental data (symbols) are from Ref. [24].

The light-fragment mass number around potential-energy minimum is around $A_L = 96$ ($A_H = 140$), corresponding to the peak region of yield distribution of fission fragment. The deformation parameters values of β_{2i} and β_{3i} change

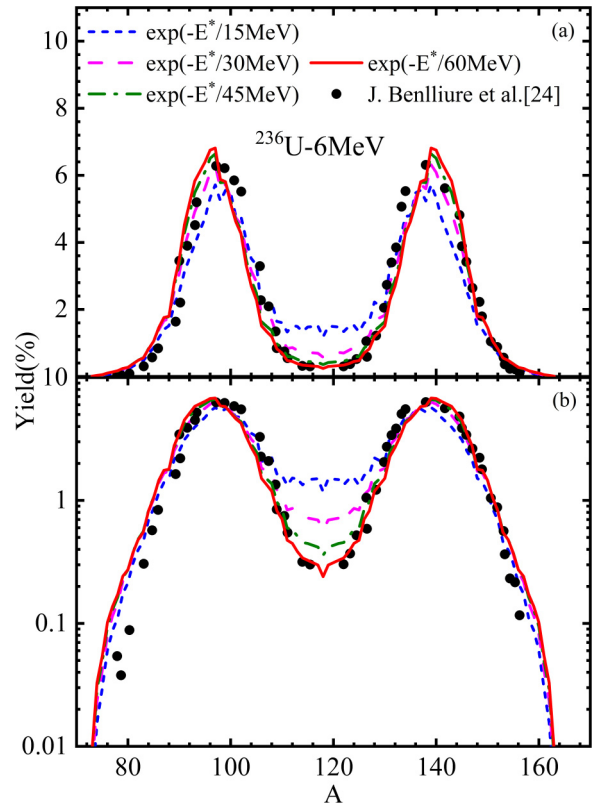

FIG. 5. The calculated mass distributions for fission of ^{235}U by neutron induced as a function for various values of the damping energy E_D (indicated in MeV) in liner (a) and logarithmic (b) coordinates. The experimental data (symbols) are from Ref. [24].

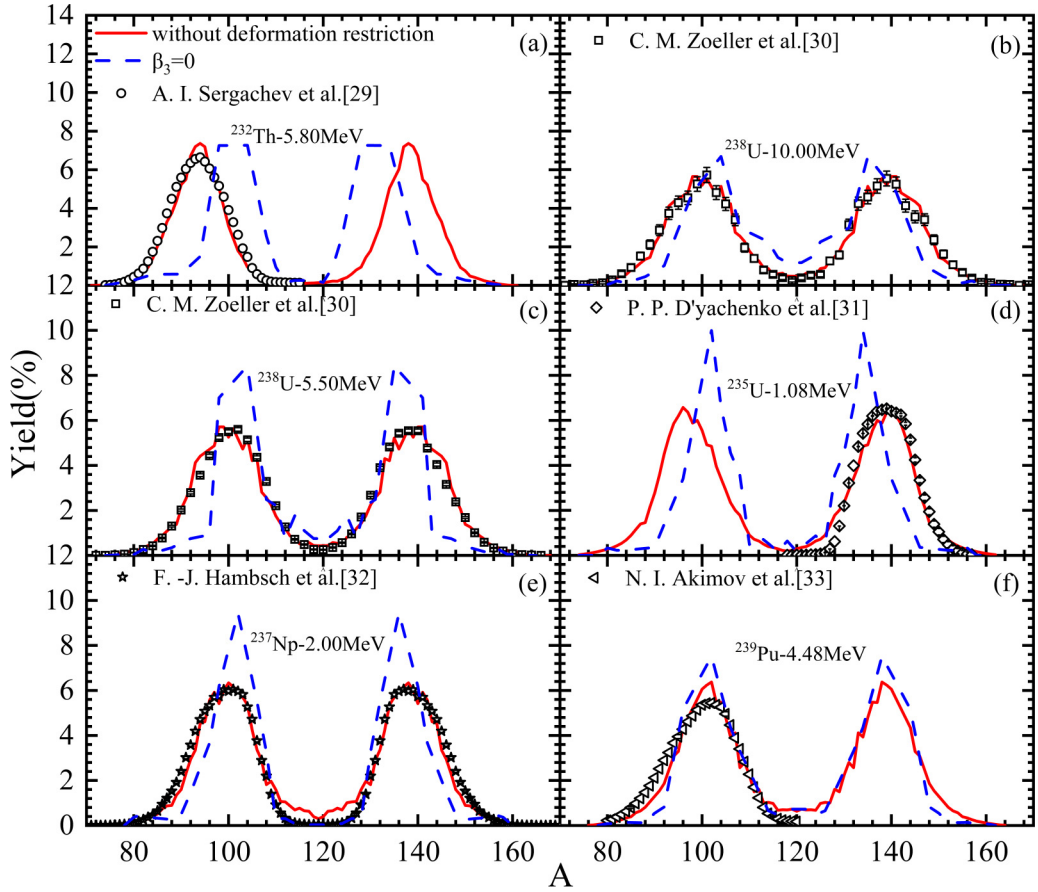

FIG. 6. The calculated mass distributions at $\beta_3 = 0$ (blue dashed line) and without deformation restriction (red c line) for fission of (a) ^{232}Th, (b) and (c) ^{238}U, (d) ^{235}U, (e) ^{237}Np, and (f) ^{239}Pu by neutron induced with incident energies of 5.80, 10.00, 5.50, 1.08, 2.00, and 4.48 MeV are compared with the experimental data from Refs. [29–33].

from 0.0 to 0.5 in steps of 0.05. Comparison of the shell energies with $\beta_3 = 0$ and without deformation restriction (β_{2i} and β_{3i} change from 0.0 to 0.5 in steps of 0.05) shows that the spherical shell gaps at $A_L = 102$–104 ($A_H = 132$–134) diminish impact, whereas, the influence of other shell gaps at $A_L = 94$–98 ($A_H = 138$–142) significantly increase with increasing octupole deformation. Thus, considering octupole deformation of heavy fragments, it shows the transformation in the region of minimum potential energy. In the fission of ^{236}U, the formation in the ^{140}Xe region is more favorable. We can obtain the mass distribution with a maximum in the ^{140}Xe region, which is an agreement with the experimental results. This confirms the strong effects of octupole effects associated with the asymmetric fission.

Figures 3(a) and 3(b) show most probable quadrupole and octupole deformations of light and heavy fragments as a function of mass number. We can see that the scission configurations are characterized by small quadrupole deformation of heavy fragments and large quadrupole deformation of light fragments. The octupole deformations of light fragments remain around 0.4 and the heavy fragments remain 0.2–0.25. Both fragments have significant quadrupole and octupole deformations. These octupole deformations are not surprising since the pear shape is caused by the neck where there is still strong nuclear attraction between the before scission. In 2019, Scamps and Simenel [16] raised the heavy fragments of ^{236}U fission have octupole deformation parameters $\beta_3 \approx 0.25 \pm 0.02$ and light fragments have octupole deformation with $\beta_3 \approx 0.3 \sim 0.4$ at scission ($\sim$0.1 zs before the neck breaks) based on constrained and time-dependent Hartree-Fock with Bardenn-Cooper-Schrieffer dynamical pairing correction. This conclusion is also confirmed by our results.

Figure 3(c). shows the relationship between the octupole deformations of heavy fragments and the interaction potential energy. In the case of only the nuclear potential ($V_C = 0$), there is no octupole deformations of heavy fragments and nearly spherical in shape, which can maintain relatively compact distance. Under the action of Coulomb potential only ($V_N = 0$), the heavy fragments have large octupole deformations. In the absence of interaction potential ($V_C = V_N = 0$), the heavier fragments ($A_H \geqslant 140$) have octupole deformations, which indicates that these nuclei are octupole deformed in ground state. This is mutually verified with the conclusion of shell effect in Fig. 1. Taking into account the interaction potential ($V_C \neq V_N \neq 0$), these nuclei all obtain octupole deformation. Therefore, we can deduce that the octupole deformations come from the interaction potential between two fragments.

IV. RESULTS AND DISCUSSION

Figure 4 shows the calculated mass distributions of ^{235}U(n, f) at $\beta_3 = 0$ (blue dashed line) and without deformation restriction (β_{2i} and β_{3i} change from 0.0 to 0.5 in steps of 0.05) (red solid line), which are compared with experimental data at the incident-neutron-energy 6 MeV [24]. The peak position of the calculated mass distributions without deformation restriction is in good agreement with the experimental. As well as light fragments have also octupole deformation and can reduce corresponding potential-energy surface, which results in a larger yields and wider distribution of the corresponding light fragments not underestimates the mass yields for $A_L < 94$ [25]. As mentioned above, our results show that the more probable scission configuration is the pear-shaped heavy fragments of ^{140}Xe rather than more spherical shape of ^{132}Sn. The most important features of fission nuclear shape, such as elongation and reflection asymmetry, are described by quadrupole and octupole deformation [26,27]. We can infer that the dynamical fission paths will eventually reach the minima related to asymmetric pear shaped on the potential-energy surface. We also calculated the mass distribution at $\beta_{3L} = 0.4$, $\beta_{3H} = 0.2$ of ^{235}U(n, f) (red solid line).

The mass asymmetry depends on the contribution of shell correction. The damping factor E_D describes the speed of washing out the shell correction relative to the excitation energy. However, the damping constant E_D is not a constant value, depending on excitation energy (temperature), which can vary from $E_D = 15$ MeV to $E_D = 60$ MeV [28]. In this paper, we only consider the case of low-energy induced fission. Therefore, for the sake of simplicity, setting a constant damping constant value is feasible. Figure 5 shows the calculated mass distributions for a wide range of damping energies E_D in liner and logarithmic coordinates and compare with the experimental data. It is obvious that E_D in the range of 15–45 MeV are too small, leading to a large peak-to-valley ratio. The experimental data are well reproduced for $E_D = 60$ MeV. Therefore, we use the $E_D = 60$ MeV for subsequent calculations.

To verify the model description, Fig. 6 shows the calculated mass distributions for neutron-induced ^{232}Th ^{235,238}U, ^{238}U, ^{237}Np, and ^{239}Pu fission, compared with $\beta_3 = 0$. The results of considering the octupole deformation are in better agreement with the experimental data [29–33] especially the peak position for ^{232}Th(n, f) reaction. This suggests the peak position of mass distributions is dominantly driven by octupole deformation shell effects.

Figure 7 shows the calculated neutron-charge ratio (neutron excess) for ^{236,239}U and ^{240}Pu fission. The results are described by scission point model (red solid line), which agree well with the experimental data at 8.3 MeV [34], and macroscopic LD model (blue dashed line). It shows that the N/Z ratios are all around the expectation of the macroscope model prediction. The deviation from the macroscope prediction is the contribution of the shell effects. The sawtooth structure relates to the shell structure of fragments. In the case of fissioning ^{236}U, the most probable configuration at $Z_L = 32$ is ^{82}Ge + ^{154}Nd due to the closed shell $N_L = 50$. And the probable macroscope configuration is ^{81}Ge + ^{155}Nd. The

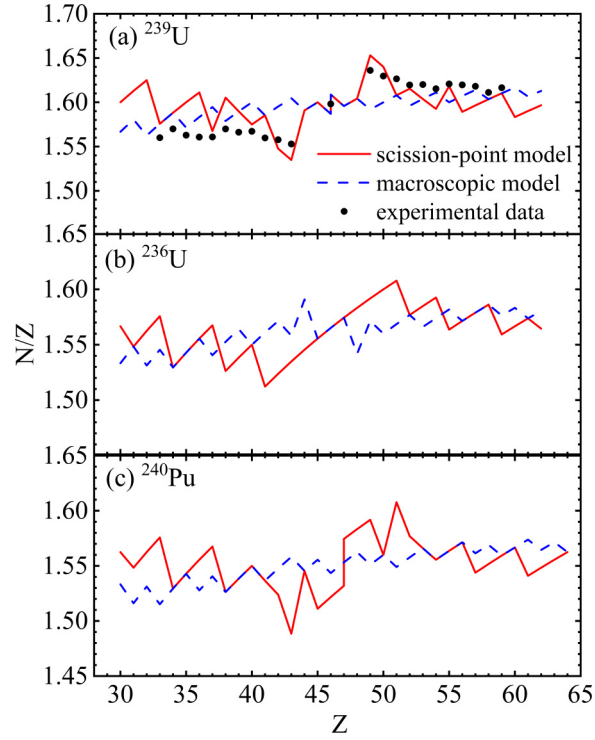

FIG. 7. The neutron-charge ratio for (a) ^{239}U, (b) ^{236}U, and (c) ^{240}Pu fission by the scission point model (red solid line) and macroscopic LD model (blue dashed line). The experimental data (symbols) are from Ref. [34].

configuration ^{92}Kr + ^{144}Ba, ^{96}Sr + ^{140}Xe, and ^{103}Nb + ^{133}Sb become the most likely due to the neutron shells $N_H = 82$, 86, and 88 of heavy fragments. In the intervals $Z_L = 40$ and 41, the neutron number of heavy fragments is close to magic 82 and almost unchanged. Therefore, the ratio decreases with increasing Z. These suggest the octupole and quadrupole deformation shell effects of the fragments strongly impact the neutron-charge ratio.

Low-energy fission in the actinide region is asymmetric. These results are first traced back to the main effect of the number of shell-stabilized neutrons in nascent fragments. In the year 2000, advances in experimental methods made it possible to obtain the charge number distribution. These experimental results may indicate that the shell effects in proton number play a more important role in asymmetric fission thought previously. Simultaneously, to further the role of shells in the asymmetric split in the actinides, the $Z_{L(H)}$ and $N_{L(H)}$ are shown in Fig. 8 as a function of $Z_{\rm CN}/A_{\rm CN}$ and $N_{\rm CN}$. The experimental data include both (γ, f) reaction [35,36] and neutron-induced fission [29–33]. In this case, the $Z_{L(H)}$ and $N_{L(H)}$ are the mean number from a multi-Gaussian fit of the experimental distribution and derived under the unchanged-density assumption: $N_H = N_{\rm CN} \times Z_{\rm H}/Z_{\rm CN}$. Our calculated values indicate that the charge number of heavy fragment is constant at $Z_H = 54$, and the experimental data are also confined within a narrow range around 54. On the contrary, the light fragment charge is much more dependent on $Z_{\rm CN}/A_{\rm CN}$. This confirms that the asymmetric fission mode

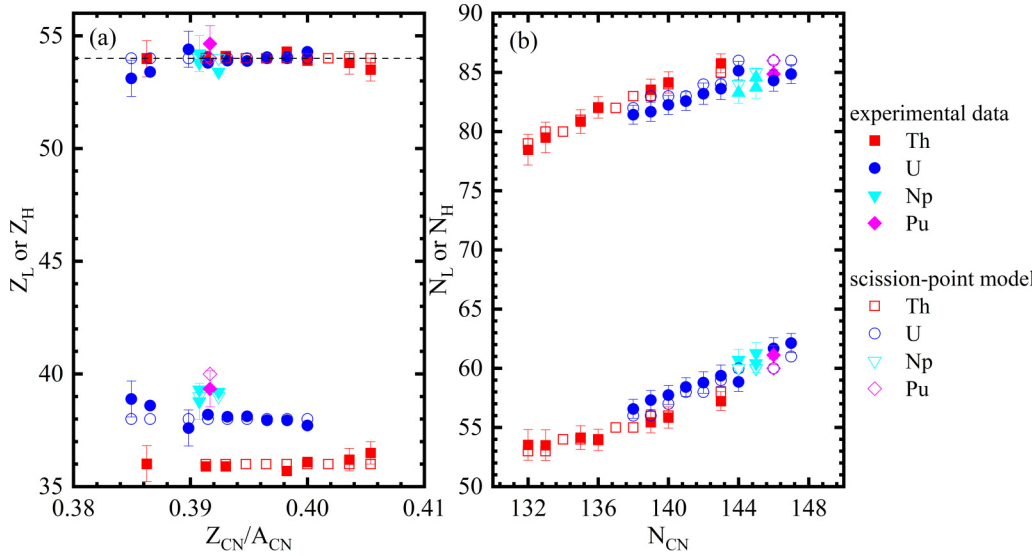

FIG. 8. The peak position of light and heavy fragments in (a) charge number $Z_{L(H)}$ and (b) neutron number $N_{L(H)}$ as a function of Z_{CN}/A_{CN} and N_{CN}.

"$Z_H \approx 54$" play a major role in the population of the fission fragments in actinides fission. The both N_L and N_H increase with increasing number of neutrons N_{CN}. We can deduce that protons configuration of heavy fragment plays a dominant role in asymmetric fission of actinides.

The difference between experimental and theoretical values of $Z^{exp}_{L(H)} - Z^{th}_{L(H)}$ and $N^{exp}_{L(H)} - N^{th}_{L(H)}$ are shown in Fig. 9 as a function of Z_{CN}/A_{CN} and N_{CN}. The differences of the peak of charge number distribution do not exceed 0.89 nucleons, and neutron number do not exceed 1.14 nucleons. Because the peak position of neutron distribution is derived under the unchanged-density assumption anther than experimentally measured directly, which leads to some error. On the whole, the calculated results are in good agreement with experimental data within the error range.

V. CONCLUSION

In this paper, we calculated the mass yields and neutron-charge ratio of actinides fission based on the improved

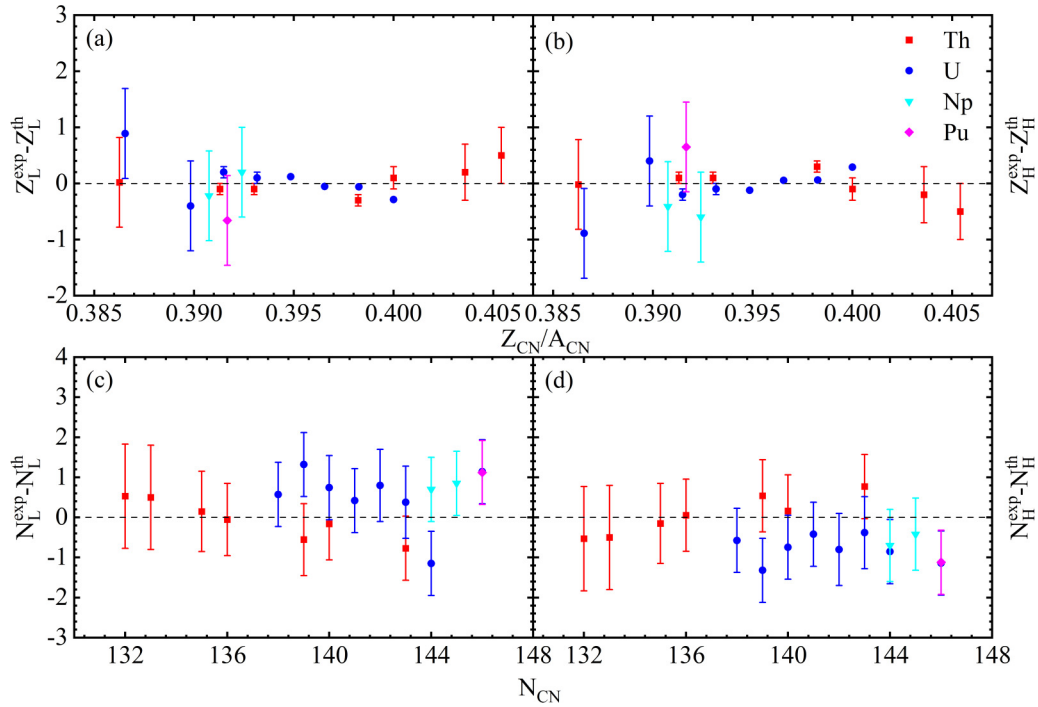

FIG. 9. The peak position of the difference between experimental and theoretical values of light and heavy fragments in (a) and (b) charge number $Z_{L(H)}$ and (c) and (d) neutron number $N_{L(H)}$ as a function of Z_{CN}/A_{CN} and N_{CN}.

scission point model, which results in good agreement with the experiments results. Knowledge of deformation of fragments plays a crucial role at the scission point. Compared with previous work, we introduce octupole deformation to describe the shape of fragments.

The scission point model is improved by considering the octupole deformations of the fission fragments, which can accurately calculate the mass distributions of neutron-induced actinides fission with low incident neutron energy. The heavy fragments peak position of mass distributions tends to ^{140}Xe region, it can be concluded that the octupole deformation plays an important role on the way to fission, which strongly inhibits the impact of spherical shell effect at the scission point.

The improved scission point model can also calculate the neutron-charge ratio (neutron excess) of actinides fission, the octupole and quadrupole deformation shell effects of fragments jointly impact the neutron-charge ratio. Moreover, the improved scission point model can also account for the constant proton number for actinides in the fission process, which is approximately constant at $Z \approx 54$. We deduce that protons configuration of heavy fragment plays a dominant role in asymmetric fission of actinides.

The improved scission point model considers the octupole deformations of the fission fragments, which show a significant advance for calculating yields of neutron-induced typical actinides fission. More importantly, pear-shaped fission fragments described by the improved scission point model can driver for the formation of the heavy fragments by along with the spherical shell effects, which is expected to further understand the fission process.

ACKNOWLEDGMENTS

This work was supported by the NSFC-Nuclear Technology Innovation Joint Fund (Grants No. U2167203 and No. U1867213), the National Natural Science Foundations of China (Grant No. 12075105), and the Fundamental Research Funds for the Central Universities (Grants No. lzujbky-2022-kb07 and No. lzujbky-2022-ey14).

[1] L. Audouin, E. Pellereau, J. Taieb, G. Boutoux, G. Béliera, A. Chatillon, A. Ebran, T. Gorbinet, B. Laurent, J.-F. Martin, L. Tassan-Got, B. Jurado, H. Alvarez-Pol, Y. Ayyad, J. Benlliure, M. Caamano, D. Cortina-Gil, B. Fernandez-Dominguez, C. Paradela, J.-L Rodriguez-Sanchez, J. Vargas, E. Casarejos, A. Heinz, A. Kelic-Heil, N. Kurz, C. Nociforo, S. Pietri, A. Prochazka, D. Rossi, K.-H. Schmidt, H. Simon, B. Voss, H. Weick, and J. S. Winfield, in *Nuclear Physics and Gamma-Ray Sources for Nuclear Security and Nonproliferation* (World Scientific, 2014), pp. 217–225.

[2] B. D. Wilkins, E. P. Steinberg, and R. R. Chasman, Phys. Rev. C **14**, 1832 (1976).

[3] P. Fong, Phys. Rev. **135**, B1338 (1964).

[4] H. Pasca, A. V. Andreev, G. G. Adamian, and N. V.Antonenko, Phys. Rev. C **104**, 014604 (2021).

[5] H. Paşca, A. V. Andreev, G. G. Adamian, and N. V. Antonenko, Phys. Rev. C **101**, 064604 (2020).

[6] H. Paşca, A. V. Andreev, G. G. Adamian, and N. V. Antonenko, Phys. Rev. C **99**, 064611 (2019).

[7] H. Pasca, A. V. Andreev, G. G. Adamian, and N. V. Antonenko, Nucl. Phys. A **969**, 226 (2018).

[8] J.-F. Lemaître, S. Panebianco, J. L. Sida, S. Hilaire, and S. Heinrich, Phys. Rev. C **92**, 034617 (2015).

[9] J.-F. Lemaître, S. Goriely, S. Hilaire, and J. L. Sida, Phys. Rev. C **99**, 034612 (2019).

[10] H. Pasca, A. V. Andreev, G. G. Adamian, and N. V. Antonenko, Phys. Rev. C **97**, 034621 (2018).

[11] A. V. Andreev, G. G. Adamian, and N. V. Antonenko, Phys. Rev. C **86**, 044315 (2011).

[12] A. V. Andreev1, G. G. Adamian1, N. V. Antonenko1, S. P. Ivanova, and W. Scheid, Eur. Phys. J. A **22**, 51 (2004).

[13] B. Bucher, S. Zhu, C. Y.Wu, R. V. F. Janssens, D. Cline, A. B. Hayes, M. Albers, A. D. Ayangeakaa, P. A. Butler, C. M. Campbell, M. P. Carpenter, C. J. Chiara, J. A. Clark, H. L. Crawford, M. Cromaz, H. M. David, C. Dickerson, E. T. Gregor, J. Harker, C. R. Hoffman, B. P. Kay, F. G. Kondev, A. Korichi, T. Lauritsen, A. O. Macchiavelli, R. C. Pardo, A. L. Richard, M. A. Riley, G. Savard, M. Scheck, D. Seweryniak, M. Smith, R. C. Vondrasek, and A. Wiens, Phys. Rev. Lett. **116**, 112503 (2016).

[14] B. Bucher, S. Zhu, C. Y. Wu, R. V. F. Janssens, R. N. Bernard, L. M. Robledo, T. R. Rodriguez, D. Cline, A. B. Hayes, A. D. Ayangeakaa, M. Q. Buckner, C. M. Campbell, M. P. Carpenter, J. A. Clark, H. L. Crawford, H. M. David, C. Dickerson, J. Harker, C. R. Hoffman, B. P. Kay, F. G. Kondev, T. Lauritsen, A. O. Macchiavelli, R. C. Pardo, G. Savard, D. Seweryniak, and R. Vondrasek, Phys. Rev. Lett. **118**, 152504 (2017).

[15] L. P. Gaffney, P. A. Bulter, M. Scheck, A. B. Hayes, F. Wenander, M. Albers, B. Bastin, C. Bauer, A. Blazhev, S. Bönig, N. Bree, J. Cederkäll, T. Chupp, D. Cline, T. E. Cocolios, T. Davinson, H. De Witte, J. Diriken, T. Grahn, A. Herzan, M. Huyse, D. G. Jenkins, D. T. Joss, N. Kesteloot, J. Konki, M. Kowalczyk, Th. Kröll, E. Kwan, R. Lutter, K. Moschner, P. Napiorkowski, J. Pakarinen, M. Pfeiffer, D. Radeck, P. Reiter, K. Reynders, S. V. Rigby, L. M. Robledo, M. Rudigier, S. Sambi, M. Seidlitz, B. Siebeck, T. Stora, P. Thoele, P. Van Duppen, M. Vermeulen, M. von Schmid, D. Voulot, N. Warr, K. Wimmer, K. Wrzosek-Lipska, C. Y. Wu, and M. Zielinska, Nature (London) **497**, 199 (2013).

[16] G. Scamps and C. Simenel, Nature (London) **564**, 382 (2018).

[17] N. Wang, M. Liu, and X. Wu, Phys. Rev. C **81**, 044322 (2010).

[18] X. H. Ruan, J. T. Hu, and T. Rong, J. Phys. G: Nucl. Part. Phys. **46**, 125108 (2019).

[19] D. Y. Huo, X. Yang, and C. Han, Chin. Phys. C **45**, 132 (2021).

[20] V. M. Strutinsky and F. A. Ivanjuk, Nucl. Phys. A **255**, 405 (1975).

[21] C. Y. Wong, Phys. Rev. Lett. **31**, 766 (1973).

[22] H. Pasca, A. V. Andreev, G. G. Adamian, N. V. Antonenko, and Y. Kim, Phys. Rev. C **93**, 054602 (2016).

[23] W. Urban, T. Rzaca-Urban, and N. Schulz, Eur. Phys. J. A **16**, 303 (2003).

[24] J. Benlliure, A. Grewe, M. de Jong, K.-H. Schmidta, and S. Zhdanov, Nucl. Phys. A **628**, 458 (1998).

[25] H. Pasca, A. V. Andreev, G. G. Adamian, and N. V. Antonenko, Phys. Lett. B **760**, 800 (2016).
[26] A. Bulgac, S. Jin, K. Roche, N. Schunck, and I. Stetcu, Phys. Rev. C **100**, 034615 (2019).
[27] M. Warda, K. Pomorski, and J. L. Egido, Phys. G: Nucl. Part. Phys. **31**, S1555 (2005).
[28] F. A. Ivanyuk, C. Ishizuka, and M. D. Usang, Phys Rev C **97**, 054331 (2018).
[29] A. I. Sergachev, V. G. Vorob'Eva, B. D. Kuz'Minov, V. B. Mikhaylov, and M. Z. Tarasko, Yad. Fiz. **7**, 778 (1968).
[30] C. M. Zoeller, A. Gavron, J. P. Lestone, M. Mutterer, and J. P. Theobald, *Seminar on fission "Pont d'Oye III", Castle of Pont d'Oye, Habay-la-Neuve, Belgium* (1995), p. 56.
[31] P. P. D'yachenko, B. D. Kuz'minov, and M. Z. Tarasko, Yad. Fiz. **8**, 286 (1968).
[32] F. -J. Hambsch and F. Vivès, Nucl. Phys. A **679**, 3 (1999).
[33] N. I. Akimov and Vorob'eva, Yad. Fiz. **13**, 484 (1971).
[34] D. Ramos, M. Caamaño, A. Lemasson, M. Rejmund, H. Alvarez-Pol, L. Audouin, J. D. Frankland, B. Fernández-Domínguez, E. Galiana-Baldó, J. Piot, C. Schmitt, D. Ackermann, S. Biswas, E. Clement, D. Durand, F. Farget, M. O. Fregeau, D. Galaviz, A. Heinz, A. Henriques, B. Jacquot, B. Jurado, Y. H. Kim, P. Morfouace, D. Ralet, T. Roger, P. Teubig, and I. Tsekhanovich, Phys. Rev. C **101**, 034609 (2020).
[35] A. Chatillon, J. Taïeb, A. Heinz, H. Alvarez-Pol, L. Audouin, Y. Ayyad, G. Bélier, J. Benlliure, G. Boutoux, M. Caamaño, E. Casarejos, D. Cortina-Gil, A. Ebran, F. Farget, B. Fernández-Domínguez, T. Gorbinet, L. Grente, H. T. Johansson, B. Jurado, A. Kelic-Heil, N. Kurz, B. Laurent, J.-F. Martin, C. Nociforo, C. Paradela, E. Pellereau, S. Pietri, A. Prochazka, J. L. Rodríguez-Sánchez, D. Rossi, H. Simon, L. Tassan-Got, J. Vargas, B. Voss, and H. Weick, Phys. Rev. C **106**, 024618 (2022).
[36] K.-H. Schmidt, S. Steinhäuser, C. Böckstiegel, A. Grewe, A. Heinz, A. R. Junghans, J. Benlliure, H. -G. Clerc, M. de Jong, J. Müller, M. Pfützner, and B. Vossa, Nucl. Phys. A **665**, 221 (2000).